Novel approach for low CO_2 intensity hydrogen production from natural gas†

Julian Straus,*[a] Vidar Torarin Skjervold,[a] Rahul Anantharaman,[a] and David Berstad[a]

Hydrogen from natural gas with CO_2 capture can be a key transition technology to a low carbon energy system due to the abundance of natural gas and the possibility to increase the hydrogen production capacity quickly. However, it is necessary to achieve both a high energy efficiency and a high CO_2 capture ratio to be a viable option. The liquefaction of CO_2 is one promising separation technology as it provides the captured CO_2 in a transportable format. This paper proposes a hydrogen production process with integrated CO_2 liquefaction. Efficiencies of up to 84.7 % (based on the higher heating value) and CO_2 capture ratios of up to 97.2 % can be achieved. One advantage of the utilization of CO_2 liquefaction as separation technology is furthermore the possibility to incorporate a partial recycle of the flue gas from the separation to the water–gas shift reaction without additional equipment, increasing both energy efficiency and carbon capture ratio.

1 Introduction

Hydrogen as energy carrier based on low-carbon energy sources is expected to play an important role in a carbon constrained energy system of the future. Several industrial and energy sectors can be partially or even fully converted to hydrogen, with the potential to reduce global CO_2 emissions substantially. In the 2050 vision of the Hydrogen Council, 18 % of the global end-use energy demand (78 EJ, corresponding to about 550 Mt of hydrogen) is supplied from hydrogen, reducing annual CO_2 emissions by 6 Gt CO_2eq[1]. The report *Net Zero by 2050*[2], released by the IEA in 2021, also highlighted the role of hydrogen in a decarbonised energy system utilizing energy system models with a production of more than 500 Mt of hydrogen in 2050. A recent European study[3] highlighted as well the importance of hydrogen especially in hard-to-abate sectors with a total consumption of around 100 Mt of hydrogen in Europe alone. Both renewables and decarbonised fossil fuels can enable hydrogen production and use with very low net CO_2 emissions and are used in the aforementioned studies.

Hydrogen supply is a major global business, with an annual demand of 70 Mt/a purified hydrogen (primarily in the refining and ammonia industry) and additionally 45 Mt/a crude hydrogen[4] (use of hydrogen as a component of synthesis gas in, *e.g.* , methanol synthesis or direct reduction of iron). Hydrogen supply has increased significantly in the last two decades[5]. Since fossil energy sources dominate the hydrogen production industry, the resulting CO_2 emissions caused by hydrogen production are currently 830 Mt CO_2eq/a[4]. There has thus been a focus on identifying efficient, scalable technologies for hydrogen production from fossil fuels with low emissions, where the hydrogen production process is realised with CO_2 capture and storage[6]. Hydrogen from natural gas can reach parity with hydrogen from renewable power provided that the overall CO_2 capture ratio (CCR) is sufficiently high and upstream emissions of natural gas sufficiently low[7]. While the oil and gas industry is responsible for reducing the upstream emissions associated to natural gas production and methane leakage, it is the task of the process industry for achieving a high CO_2 capture ratio. This requires an adequate combination of conversion and separation technologies.

A first focus is the reforming reactor type. The main reforming reactors are steam methane reformer (SMR), autothermal reformer (ATR), and gas heated reformer (GHR)[8]. SMRs are used today and require an external heat source for providing energy to the endothermic reaction. Heat can be also provided from inside the reactor in an ATR, having the advantage that all produced CO_2 is present in a single stream. GHRs are similar to SMRs but the required heat is provided through a gas stream and not a combustion reaction. Hence, they are frequently coupled with ATRs. Novel reactor technologies like protonic membrane reactors (PMR) are also developed[9] and combine both reforming and hydrogen separation. PMRs can be coupled with CO_2 separation and purification[10]. Another approach is the gas switching reformer (GSR), a cyclic approach of a chemical looping reactor[11]. This reactor type utilizes a cyclic approach for combining methane reforming and CO_2 capture in a single reactor. An overview of the different reactor technologies is provided by Voldsund *et al.* [12].

The hydrogen separation technology plays an important role in addition to the methane conversion reactor. Pressure swing adsorption (PSA) is the standard technology for hydrogen separation from syngas[13]. Hydrogen selective membranes offer an energy efficient alternative to PSA particularly for hydrogen production with CO_2 capture. Hydrogen membranes and membrane reactors have been an active area of research for low emission hydrogen production from fossil fuels with CO_2 capture[14]. Dense metal membranes (mainly palladium alloys) and dense ceramic membranes are currently the most suitable materials to produce high purity hydrogen streams. Palladium alloy membranes, with their high hydrogen permeability, mechanical durability, and in some cases resistance to impurities have shown their potential to be a cost-efficient alternative[15].

A CO_2 separation or purification step is required to achieve CO_2 at transport purity and conditions. Absorption is the most commonly used process today for separating CO_2 from a gas

[a] *Address, SINTEF Energy Research, Kolbjørn Hejes vei 1B, Trondheim 7491, Norway. E-mail: julian.straus@sintef.no*

† Electronic Supplementary Information (ESI) available: See DOI: 10.1039/D2SE00862A.

stream. CO_2 capture ratios above 98 % are achievable through rigorous process design[16], although conditioning of the captured CO_2 is required for transport. Using autothermal reforming as conversion technology, the CO_2 concentration is high at a high stream pressure (when using hydrogen selective membranes) or low stream pressure (when using PSA separation). A low–temperature liquefaction process is the best suited separation process for these conditions that produces CO_2 at high purity and allows flexibility in attaining transport conditions suitable for either pipeline or ship transport of CO_2[17]. Additionally, the low–temperature liquefaction process recovers additional hydrogen from the retentate stream. This combination of processes has been shown to be highly efficient for high purity hydrogen production with CO_2 capture from coal gasification[18].

The low–temperature CO_2 liquefaction process results in a tail gas stream at a relatively high pressure (> 30 bar). This tail gas stream is rich in CO thus reducing the CO_2 capture ratio of the overall process and increasing the CO_2 intensity hydrogen production process. This tail gas stream can potentially be recycled to the water–gas shift reactor without requiring any additional equipment. This results in an improved utilization of the natural gas feed as less hydrogen is burned for power generation. Furthermore, recycling CO_2 may result in a reduced CO_2 intensity of hydrogen if the capture ratio *per pass* is kept constant.

This paper will present based on the observation of a CO rich tail gas stream a novel process for hydrogen production from natural gas with a very low CO_2 intensity with either palladium alloy membranes or a PSA unit for hydrogen separation and low–temperature CO_2 liquefaction for CO_2 separation. It will focus on the impact of tail gas recycle to the water–gas shift reactor on both efficiency and CO_2 capture ratio for highlighting a simple approach for achieving improved capture ratios while simultaneously increasing the energy efficiency. Tail gas recycling can be seen as well as an option for other separation technologies, although its exact impact may be depending on the composition of the tail gas stream after both separation steps.

Section 2 describes the process configuration for hydrogen production, with a focus on the CO_2 sequestration process through liquefaction. Section 3 shows the detailed analysis of the impact of tail gas recycle on both the economic and environmental performance of the process, as well as the improved performance of the CO_2 sequestration process. Section 4 discusses the implication of the utilization of low temperature liquefaction as CO_2 sequestration technology. The paper concludes in Section 5.

2 Process description

2.1 General considerations

The H_2 plant is designed for a production capacity of 450 t/d of H_2 at a pressure of 20 bar in the configuration using the palladium membrane process and a pressure of 34 bar in the configuration using pressure swing adsorption (the outlet pressure of the adsorption unit). The pressure of 20 bar corresponds to the most common feed conditions for H_2 liquefaction. The sequestered CO_2 is delivered at a pressure of 110 bar and is required to have a temperature below 30 °C. The process was modelled in Aspen HYSYS. All reactors, except for the tail gas furnace, were modelled as equilibrium reactors. The latter was modelled as a Gibbs reactor. The heat exchangers were modelled as simple end–point heat exchangers. The following sections will describe the process sections and list the main modelling assumptions. Table 1 provides an overview of the general process parameters used for all unit operations in the paper.

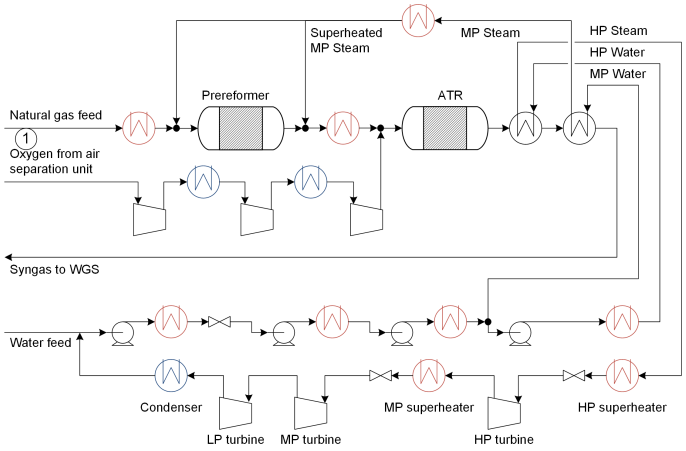

Fig. 1 Reforming section, consisting of a prereformer and an autothermal reformer (ATR), with steam cycle. Red labelled heat exchangers correspond to heaters, whereas blue labelled heat exchangers correspond to coolers. The reader is referred to the web version for colour coding.

2.2 Reforming section and steam cycle

The reforming section is the core section for the production of H_2 and is an oxygen-blown autothermal (ATR) reforming process, where O_2 is supplied by a conventional cryogenic air separation unit. The layout of the air separation unit has not been considered and for simplicity, it is assumed that the O_2 is supplied at atmospheric pressure and compressed to the reaction pressure in a three-stage intercooled compression train. A process flow diagram of the reforming section can be found in Fig. 1. The reforming of the natural gas is performed in two steps. First, the natural gas feed is preheated, mixed with superheated medium pressure (MP) steam, and fed to a prereformer to convert higher hydrocarbons to CH_4, H_2, CO, and CO_2 according to the follow-

Table 1 General process parameters

Parameter	Value	Unit
Mechanical to electrical efficiency	0.98	–
Cooling water pump power demand	0.007	$\frac{kW_{el}}{kW_{th}}$
Cooling water inlet temperature	10	°C
Pump efficiency	80	%
Isentropic efficiency compressors	85	%
Isentropic efficiency expanders	85	%

ing reactions:

$$CH_4 + H_2O \rightleftharpoons CO + 3H_2 \quad (1)$$

$$C_2H_6 + 2H_2O \rightleftharpoons 2CO + 5H_2 \quad (2)$$

$$C_3H_8 + 3H_2O \rightleftharpoons 3CO + 7H_2 \quad (3)$$

$$C_4H_{10} + 4H_2O \rightleftharpoons 4CO + 9H_2 \quad (4)$$

$$CO + H_2O \rightleftharpoons CO_2 + H_2 \quad (5)$$

Reactions (1) to (4) correspond to reforming reactions. These reactions are all endothermic. Reaction (5) corresponds to the exothermic water-gas shift reaction which is also the governing reaction in the water-gas shift reactors. The reforming reactions for the higher hydrocarbons (C_2 and higher) result in complete conversion for C_3 and higher, while the conversion of C_2H_6 is close to 100 %. The reactor outlet contains correspondingly only 0.02 mol% C_2H_6. The reactor outlet is then mixed with superheated MP steam and O_2 from the air separation unit and fed to an autothermal reformer. The autothermal reformer converts CH_4 to H_2, CO, and CO_2 through reactions (1) and (5) with the following, additional reaction equations:

$$CH_4 + 2O_2 \rightleftharpoons CO_2 + 2H_2O \quad (6)$$

$$C_2H_6 + 3.5O_2 \rightleftharpoons 2CO_2 + 3H_2O \quad (7)$$

These two reactions correspond to combustion of the fuel to provide the energy for the endothermic reforming reactions. Reaction (7) leads to a complete combustion of the remaining C_2H_6. The reactor outlet temperature is controlled using the O_2 flowrate. The reactor outlet is cooled in two heat exchangers, first for the evaporation of high pressure (HP) water, and subsequently for the evaporation of MP water which is fed to both the prereformer and the ATR. The resulting synthesis gas is then fed to the water–gas shift section. The key process parameters for the reforming section can be found in Table 2. The used temperature levels and steam/carbon ratios for the reformer reactors are derived from the values provided by Aasberg-Petersen *et al.* [19] and direct discussions with industrial partners. The used ASU power demand is slightly below the one reported by Antonini *et al.* [20].

Table 2 Key process parameters for the reforming section and the steam cycle, adopted from Aasberg-Petersen *et al.* [19] and Antonini *et al.* [20]

Parameter	Value	Unit
Steam/Carbon – prereformer	1.5	–
Feed temperature – prereformer	410	°C
Steam/Carbon – ATR	1.5	–
Feed temperature – ATR	454	°C
Outlet temperature – ATR	1050	°C
ASU power demand	200	$\frac{kWh_{el}}{t\ O_2}$
Low pressure steam/water (LP)	4.8	bar
Medium pressure steam/water (MP)	45	bar
High pressure steam/water (HP)	126	bar

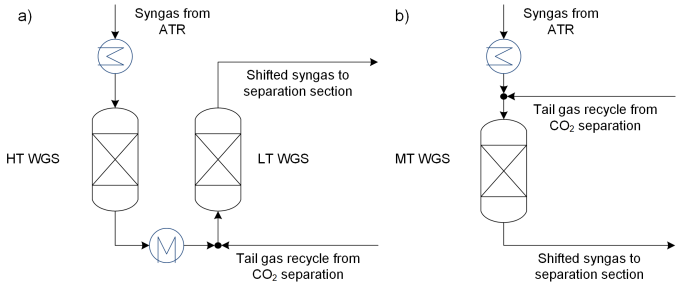

Fig. 2 Water–gas shift section consisting of a) a high temperature (HT) and low temperature (LT) water–gas shift reactor and b) a medium temperature (MT) water–gas shit reactor. Blue labelled heat exchangers correspond to coolers. The reader is referred to the web version for colour coding.

However, the exact value will only impact the reported efficiencies and not the trends as the reforming section is unaffected by the conducted analyses.

The steam cycle provides the process with MP steam and electricity and consists of three pressure levels as described in Table 2.

2.3 Water–gas shift section

The process flow diagram of the water–gas shift WGS section is illustrated in Fig. 2. Two different configurations are investigated in this study, a combination of a high temperature (HT) and a low temperature (LT) reactor, as well as a single medium temperature (MT) reactor. The latter results in an increased outlet temperature which reduces the size of the required palladium membrane in separation.

In setup a), the synthesis gas from the ATR is first cooled down and then fed to the HT WGS reactor. The reactor outlet is further cooled down, mixed with tail gas from the low temperature CO_2 liquefaction section, and fed to the LT WGS reactor. Setup b) differs as the tail gas recycle is mixed directly with the synthesis gas. Only reaction (5) takes place in the reactors. The key process parameters of the water–gas shift section can be found in Table 3.

2.4 H_2 and CO_2 separation

Two separation steps for H_2 and CO_2 separation are typically required to ensure that the purity specification for H_2 and CO_2 streams are met [12]. All investigated cases first separate H_2 selectively and subsequently CO_2. The technologies considered for H_2 separation are pressure swing adsorption (PSA), a conventional and proven technology, and palladium-alloy membranes, an emerging technology currently not fully scaled-up and com-

Table 3 Key process parameters for the water–gas shift section, adopted from Antonini *et al.* [20]

Parameter	Value	Unit
Feed temperature – HT WGS	350	°C
Feed temperature – LT WGS	200 – 300	°C
Feed temperature – MT WGS	200 – 300	°C

mercialised. CO_2 separation is achieved in all cases by condensing the CO_2 at low temperature. This is the most rational way to separate CO_2 for gas mixtures with relatively high CO_2 concentrations, particularly for the H_2/CO_2 (syngas) systems[17]. However, the choice of H_2 separation technology results in different process flow diagrams for the liquefaction section. Fig. 3 illustrates the process flow diagram for the separation section for a) palladium membrane separation and b) pressure swing adsorption separation.

As discussed earlier, the novelty of process developed and evaluated in this work is that the tail gas from the separation is partly recycled to the water–gas shift section to convert remaining CO and increase the CO_2 capture ratio while the remainder is bled from the system and burned for energy recovery. This is thus done for both the separation cases. Table 4 provides an overview of the process parameters used in the separation section. The H_2 recovery in the PSA unit is within the recovery range reported by IEAGHG[21] while the H_2 recovery rate of the Pd membrane is based on a first principle model[22]. The following subsections will describe the two different processes. Note, that with respect to the downstream processes, a key difference is in the pressure level of the product streams after separation. While pressure swing adsorption results in a low pressure CO_2 rich stream and a high pressure H_2 stream, palladium membrane separation results in a high pressure CO_2 stream and a low pressure H_2 stream, and therefore opposite H_2 and tail/retentate gas compression requirements. A modified version of the Peng-Robinson equation of state was used to simulate the separation processes as recommended by Fandiño *et al.*[23]. However, it has to be noted, that it was not possible to implement the complete reformulation of Fandiño *et al.*[23] as Aspen HYSYS does not allow temperature dependent interaction parameters. Hence, a temperature independent interaction parameter for CO_2 and H_2 was implemented.

2.4.1 H_2 separation using palladium membranes

The shifted synthesis gas is directly fed to a palladium membrane where H_2 permeates through the membrane. The membrane is selective only to H_2. The flux across the membrane is a function of the partial pressure difference of H_2 across the membrane. A lower permeate pressure reduces the size of the membrane module while a higher permeate pressure reduces the required H_2 compression. The permeate pressure is therefore an important design parameter that accounts for the aforementioned trade-off. An in-house model for the Pd membrane module was developed using Python as programming language. The membrane model is based on the development of Berstad *et al.*[22]. It has a tubular geometry and the required membrane area is calculated based on the number of equivalent pipes in a larger shell. No sweep is assumed in the separation since this would dilute the H_2 and therefore be counterproductive. Hence, the absolute pressure equals the hydrogen partial pressure on the permeate side. The permeate is subsequently compressed with interstage cooling to achieve the final desired pressure. The retentate is first cooled down to 23 °C and the condensed water is separated. The remaining water vapour is then removed using adsorptive dehydration. The CO_2 rich retentate gas is compressed in a retentate compressor and again cooled to 23 °C.

Table 4 Key process parameters for the separation section

Parameter	Value	Unit
Adsorptive dehydration power demand	3	$\frac{MJ_{el}}{kg\ H_2O}$
Tail gas recycle ratio	60 – 95	%
H_2 recovery – Pd membrane	90	%
H_2 permeate pressure	3	bar
H_2 recovery – PSA	87	%

The pressurised and dried retentate gas is further cooled using a multistream recuperative heat exchanger heat exchanger (HX1) which uses the liquefied CO_2 and the tail gas as cooling medium. A part of the CO_2 is condensed in this heat exchanger. Subsequently, it is further cooled using a propane refrigeration cycle (labelled IT auxiliary refrigeration, see Section 2.4.3) and a second multistream heat exchanger (HX2) using the tail gas, tail gas reduced in pressure through a cryoexpander, and liquefied CO_2 at two different purity levels. The cooled stream is further cooled using an ethane refrigeration loop and separated to liquid CO_2 at around 95 % purity and tail gas. The CO_2-depleted gaseous separation product is the tail gas from the low-temperature CO_2 separation unit. This tail gas is sent to HX2 for internal heat recuperation and subsequently expanded using a cryoexpander. The induced temperature reduction from the expansion allows it to be used once more in a second cold-side channel in HX2. It is thereafter used for thermal recuperation in HX1. The CO_2-rich liquid stream from the first separator is first used for heat integration in HX2 and subsequently purified in a sequence of three flash separator tanks at different pressure levels.

The cold, purified liquid CO_2 stream is compressed to supercritical pressure by a low temperature pumping stage (LT CO_2 pump) and thereafter heated in HX2 and HX1 and compressed to its final pressure by a second pumping stage (HT CO_2 pump). As the flash gas streams from the three sequential flash separation units have high CO_2 concentrations ($60-94$ mol%), they are re-compressed and mixed with the main retentate feed stream entering the low-temperature CO_2 liquefaction section. This contributes to increasing the CO_2 capture rate as well as recovering a considerable amount of valuable hydrogen and unconverted CO.

2.4.2 H_2 separation using pressure swing adsorption

The shifted synthesis gas is first cooled down to 23 °C and the condensed water separated. Subsequently, H_2 is separated using pressure swing adsorption. The pressure swing separation is not modelled in detail. Instead, it is assumed that a H_2 recovery of 87 % is achievable. As the tail gas for the pressure swing adsorption unit is at a pressure of 1.1 bar, it is necessary to compress the tail gas in five compression steps with interstage cooling. After the third stage, remaining water is removed using adsorptive dehydration. The coldbox structure is similar to the structure used in Section 2.4.1. However, as the tail gas from the PSA unit has to be compressed for liquefaction, it is not necessary to include compressors for compressing the gas stream leaving the flash sep-

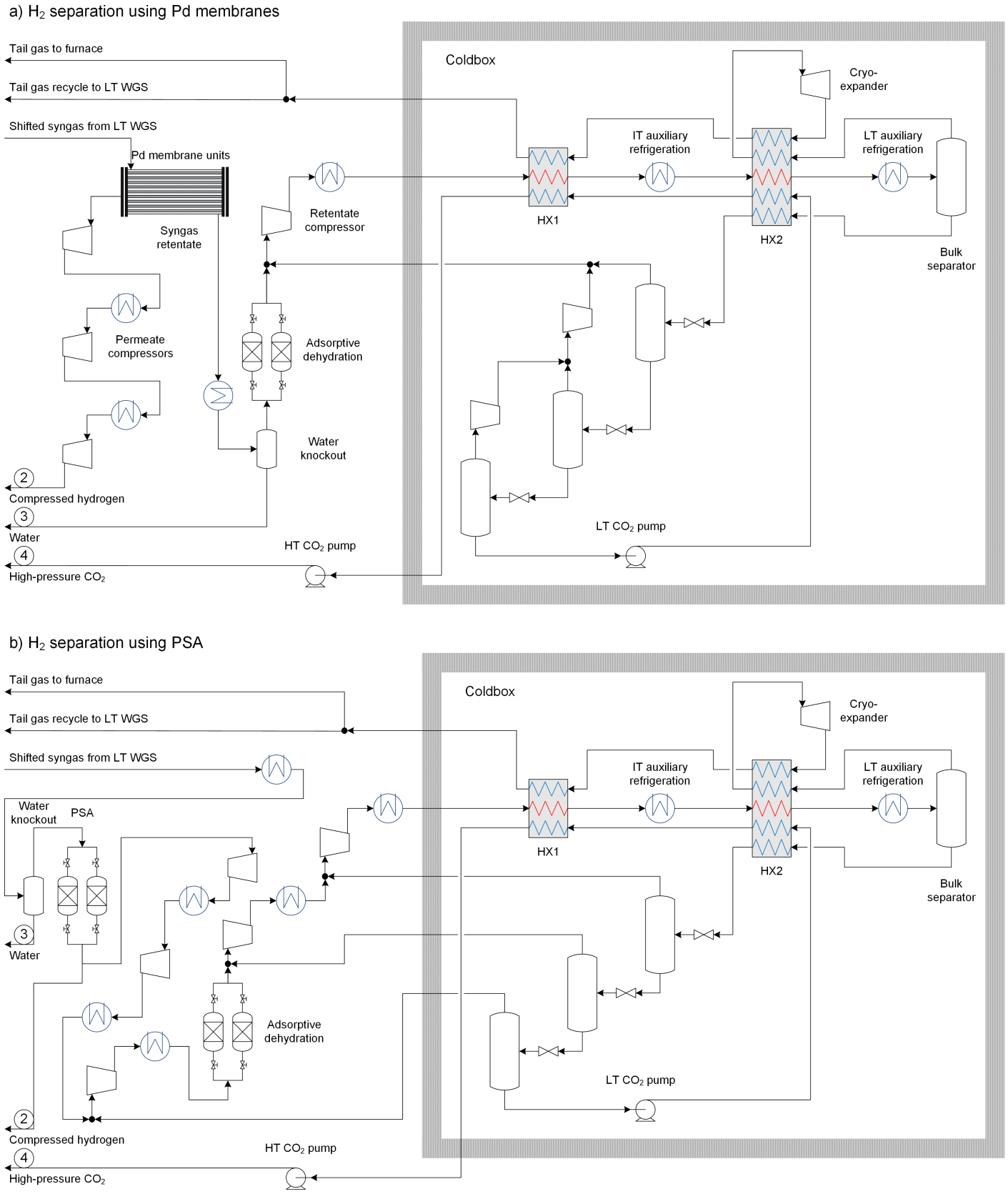

Fig. 3 H_2 and CO_2 separation using a) a palladium membrane for H_2 separation and b) a pressure swing adsorption (PSA) unit. Blue labelled heat exchangers correspond to coolers. The reader is referred to the web version for colour coding.

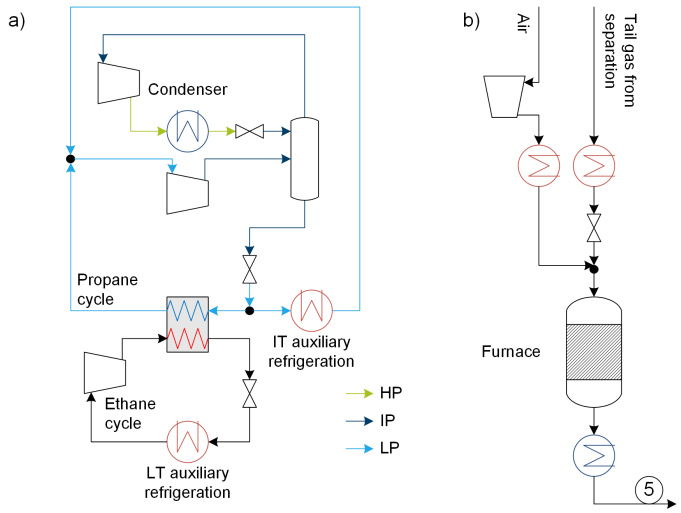

Fig. 4 a) refrigeration cycle for the liquefaction of CO_2 and b) tail gas furnace. Red labelled heat exchangers correspond to heaters, whereas blue labelled heat exchangers correspond to coolers. The reader is referred to the web version for colour coding.

arators used for purification. Instead, the gas is mixed with the feed gas at the second, third, and fourth pressure level.

2.4.3 Refrigeration cycle

The refrigeration cycle provides auxiliary cooling capacity for the liquefaction of CO_2. The structure of the refrigeration cycle is independent of the H_2 separation technology. The pressure levels may however vary in the different process configurations due to different optimal temperature levels in the liquefaction section. Fig. 4 a) illustrates the utilized configuration, which is a cascade refrigeration cycle based on single-component propane and ethane refrigerants. The intermediate temperature (IT) refrigeration cycle uses propane as refrigerant and operates at three pressure levels. The medium pressure (MP) level is compressed to the high pressure (HP) level, cooled by water, and flashed into a liquid receiver. The gas leaving the receiver is fed again to the medium–to–high pressure compressor. The liquid outlet of the receiver is further flashed to the low pressure and used for both the IT auxiliary refrigeration and the heat sink of the ethane cycle. The evaporated propane is then compressed and fed to the compressor.

The low temperature (LT) refrigeration cycle utilizes ethane as refrigerant. It has two pressure levels and utilizes the low pressure liquid propane as heat sink.

2.5 Heat integration

Heat integration of the process is done using Pinch Analysis. A global minimum temperature approach of 50 K is used in the pinch analysis. The aim of the heat integration is to maximize power generation in the steam cycle while maintaining zero hot utility demand. To this end, the steam cycle flowrate is varied. The pinch analysis was conducted using a Python script which receives all relevant parameters from the HYSYS simulation and manipulates the steam cycle flowrate directly.

2.6 Key performance indicators

Key performance indicators (KPI) are necessary for the comparison of the different process options. They consist of both environmental (*e.g.* carbon capture ratio) and efficiency (*e.g.* energy efficiency) indicators. In the following, stream 1 corresponds to the natural gas feed, stream 2 to the H_2 product stream, stream 3 to the water stream, stream 4 to the liquefied CO_2 stream, and stream 5 to the exhaust stream, as shown in Figs. 1, 3 and 4 b).

The carbon capture ratio is defined as the ratio between the molar flowrate of carbon in the captured CO_2 stream and the total carbon molar flowrate in the natural gas feed:

$$CCR = \frac{\dot{n}_{\mathrm{CO_2},4}}{\dot{n}_{C,1}} \tag{8}$$

A second important KPI related to the carbon capture ratio is the specific CO_2 emission, defined as:

$$\sigma_R = \frac{\dot{m}_{\mathrm{CO_2},3} + \dot{m}_{\mathrm{CO_2},5} + \sigma_P P_R}{\dot{m}_{\mathrm{H_2},2}} \tag{9}$$

It corresponds to the relative CO_2 emissions of the produced H_2 and is influenced by both the required electricity and its CO_2 intensity σ_P (the used value is 18.9 g/kWh and corresponds to the Norwegian electric grid in 2018) and the emitted CO_2 of the process in the water (stream 3) and furnace outlet (stream 5). Hence, the CO_2 emissions of natural gas production are not included.

The first law efficiency of the process configurations is evaluated using the energy efficiency both for the higher heating value (HHV) and the lower heating value (LHV) as:

$$\eta_R^{HHV} = \frac{HHV_{\mathrm{H_2}} \cdot \dot{m}_2}{HHV_{NG} \cdot \dot{m}_1 + P_R} \tag{10}$$

$$\eta_R^{LHV} = \frac{LHV_{\mathrm{H_2}} \cdot \dot{m}_2}{LHV_{NG} \cdot \dot{m}_1 + P_R} \tag{11}$$

P_R corresponds to the electricity input of the process. Note, that P_R is always in the denominator, independently of whether electricity is generated or consumed. If electricity is generated, it should normally be positive in the nominator instead of being negative in the denominator. This will result in a small underestimation of the efficiency, if the generated electricity is large compared to the energy of the H_2 product stream. As this is not the case for a H_2 production plant, this small error is negligible.

As the first law efficiency combines both thermal and electrical energy without accounting for their different nature, it is furthermore important to calculate the specific equivalent power input:

$$v_R = \frac{LHV_{NG} \cdot \dot{m}_1 \cdot \eta_{NG} + P_R}{\dot{m}_{\mathrm{H_2},2}} \tag{12}$$

Here, it is assumed that the natural gas is used in a combined cycle gas turbine to generate electricity with a lower heating value-based thermal efficiency of η_{NG}. Typical values for state of the art combined cycle gas turbines are depending on the power output of the turbine. They can reach values of up to $\eta_{NG} = 58 - 62$ %. The efficiency η_{NG} has a significant effect on both the absolute value of the specific power input and the optimal value in the analysis. Hence, a sensitivity analysis regarding the value will

be conducted. The specific equivalent power input will balance increased power demand with reduced natural gas demand, and hence, allows a comparison of technologies in which both change.

Another relevant KPI for comparing processes is the palladium membrane area. The two cases using palladium membrane H_2 separation will be furthermore compared using the total membrane area to investigate the impact of an increased feed temperature of the last water–gas shift reactor in comparison to a reduced CO conversion in reaction (5).

Tail gas recycling may result in an increased volumetric flowrate in the cycle consisting of the water–gas shift section (Fig. 2) and the separation section (Fig. 3). As the volumetric flowrate correlates to the required equipment sizes, and hence costs, it is important to compare changes in the flowrates as well. Key flowrates, which will be investigated, are the feed to the LT–WGS reactor, the feed to the low-temperature CO_2 liquefaction section, and the natural gas feed. All flowrates are normalized using the palladium membrane model with 60 % tail gas recycle and a feed temperature to the low temperature water–gas shift reactor of 200 °C.

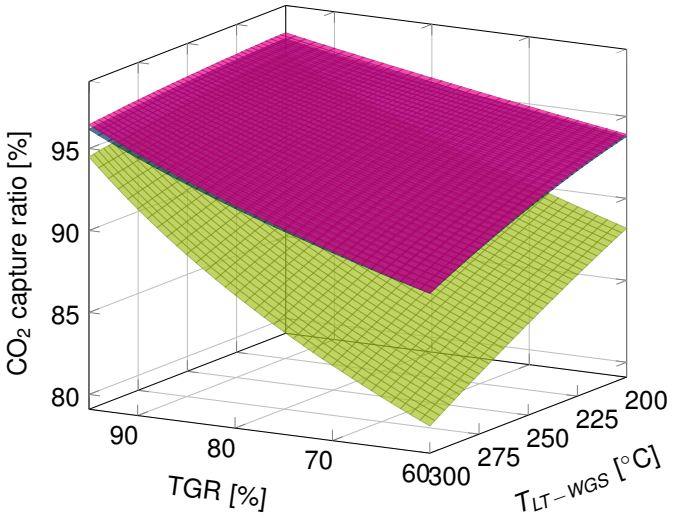

Fig. 5 CO_2 capture ratio as a function of tail gas recycle ratio (TGR) and LT–WGS inlet temperature. Process configurations 1, 2, and 3 are represented by pink, blue, and green surfaces, respectively. The reader is referred to the web version for colour coding.

3 Results

As outlined in Section 2, the three process configurations investigated in this work are:

1. pressure swing adsorption for H_2 separation as state–of–the–art H_2 separation technology with two water–gas shift reactors;

2. palladium membrane separation as novel H_2 separation technology with two water–gas shift reactors;

3. palladium membrane separation for H_2 separation with one water–gas shift reactor.

Note that all these process configurations include a low temperature CO_2 liquefaction process for CO_2 separation and purification.

3.1 Impact of tail gas recycling and WGS temperature

Tail gas recycling is a novel concept presented in this work to increase the CCR and H_2 recovery. In a first step, we analyse the impact of the tail gas recycling ratio and the feed temperature to the last water–gas shift reactor (MT or LT) on the performance of the process. To this end, a sensitivity analysis is performed in which both parameters are varied.

Fig. 5 shows that larger tail gas recycle rates result in a substantial increase in the carbon capture ratio. Lower feed temperatures to the LT–WGS are favourable, due to an increased shift of the exothermic chemical reaction towards CO_2 and H_2. Carbon capture rates of 97.4 % and 97.3 % can be achieved by process configurations 1 and 2, where both a HT–WGS and a LT–WGS reactor are present. Process configuration 3, with one MT–WGS, achieves slightly lower CCR values over most of the domain but gives a carbon capture ratio of over 97.0 % at a high recycle rate and low WGS inlet temperature. It is not surprising that the CCR increases with increasing tail gas recycle and reduced feed temperature to the water–gas shift reactor. The impact of the WGS feed temperature is however less pronounced at high tail gas recycling ratios.

From Fig. 6 it can be seen that process configuration 2 has the highest HHV efficiency, with a maximum value of 84.7 %. Increasing the tail gas recycle rate reduces the consumption of natural gas in the process as higher conversion is achieved by increasing conversion of CO and recovery of H_2. This leads to an increased efficiency. The efficiency also increases with lower WGS feed temperatures as lower WGS temperature corresponds to favourable thermodynamic conditions for increased CO conversion.

Process configurations 1 and 3 exhibit similar trends for recycle rates below 90 %. Above this value, the marginal efficiency increase of the PSA process with two WGS reactors decreases slightly, caused by the increased feed stream to the CO_2 separation section. The disadvantage of the PSA process in this respect can be explained by the increased number of compression steps which are required due to the low pressure of the PSA tail gas as shown in Fig. 3 b). Again, it is possible to identify similar trends as in Fig. 5 where the impact of the feed temperature to the WGS reactor is reduced at high recycle ratios.

Contrary to the previous figures, Fig. 7 indicates the presence of an optimal value of the tail gas recycle rate with regard to the equivalent power requirement of the process. As the tail gas recycle rate is increased, the power generated from the process decreases. However, this negative effect is counteracted by the reduced consumption of natural gas caused by recycling. For process configurations 1, 2, and 3, the minimum value of v_R is found at a recycle rate of 88, 91 and 92 %, respectively.

As noted in Section 2.6, the efficiency η_{NG} has an impact on the position of the minimum of the equivalent power requirement v_R. Hence, it is necessary to investigate the impact for the decision on best tail gas recycle ratio. Fig. 8 shows the tail gas recycle ratio (TGR) and the feed temperature to the LT–WGS reactor at which η_{NG} is minimal as a function of v_R for all process configurations.

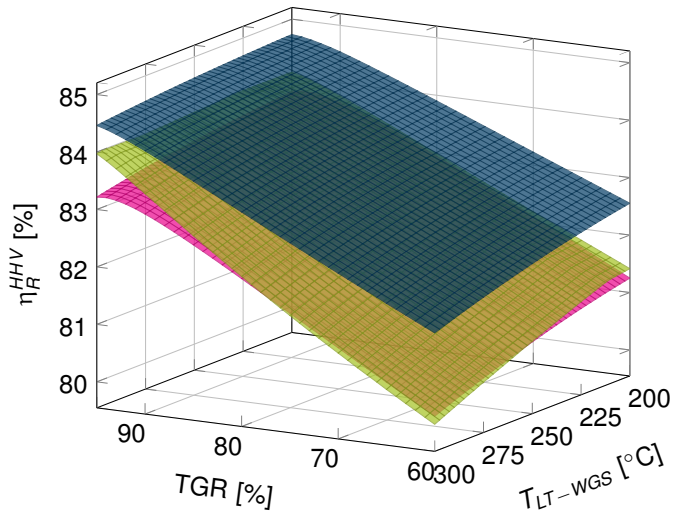

Fig. 6 Higher heating value energy efficiency as a function of tail gas recycle ratio and LT–WGS inlet temperature. Process configurations 1, 2, and 3 are represented by pink, blue, and green surfaces, respectively. The reader is referred to the web version for colour coding.

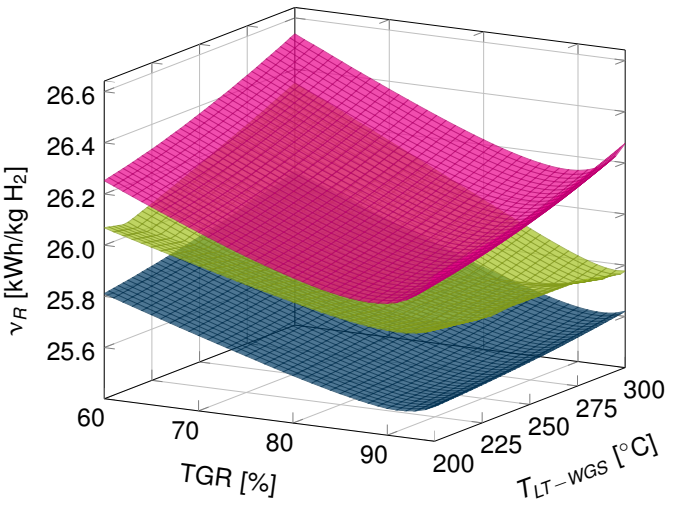

Fig. 7 Specific equivalent power input as a function of tail gas recycle ratio and LT–WGS inlet temperature with $\eta_{NG} = 60$ %. Process configurations 1, 2, and 3 are represented by pink, blue, and green surfaces, respectively. Note the rotation compared to Fig. 5 and Fig. 6. The reader is referred to the web version for colour coding.

The steps in the best tail gas recycle ratio and feed temperature is caused by the numerical tolerance of the HYSYS simulations and the changes in TGR of 1 percentage point. The figure indicates as expected that a higher η_{NG} will correspond to a higher tail gas recycle ratio for a minimum ν_R. Comparing process configurations 1 and 2, we can see that both prefer a feed temperature to the LT-WGS reactor of 200 °C independent of the chosen η_{NG}. The best tail gas recycle ratio increases however, from around 75 % to around 90 % with increased ν_R. Process configuration 2 has over the range a slightly higher best tail gas recycle ratio. Process configuration 3 behaves differently; the higher the efficiency, the higher the tail gas recycle ratio and the higher the feed temperature to the LT-WGS reactor. The first statement is expectable, although the increase is more pronounced compared to process configurations 1 and 2. The increase in the feed temperature can be explained by the increased power generation at a higher feed temperature. This counteracts in process configuration 3 the reduction in natural gas consumption.

Large gas turbines of the G or H class in a combined cycle configuration typically have an efficiency of around 60 %. Given the large natural gas requirement for a 450 t/d hydrogen production facility, $\eta_{NG} = 60$ % could be a reasonable value to use for the purposes of this work. It should however be noted that the optimal tail gas recycle ratio discussion here does not include its impact on the economics of the process. This will be discussed in Section 4.1.

From Fig. 5 and Fig. 6, we can see that the process configurations have the highest CCR and η_R^{HHV} at the lowest feed temperature to the WGS reactor. This is not surprising as a lower outlet temperature represents a higher conversion in the water–gas shift reaction, and hence a higher CO_2 and H_2 concentration in the outlet stream. ν_R behaves slightly different. Process configurations 1 and 2 have a minimum at the minimal investigated temperature for all tail gas ratios. Process configuration 3 has a minimum at a feed temperature to the MT–WGS reactor of 290 °C. Furthermore, process configuration 3 behaves slightly strange as there are local minima for a varying feed temperature. These local minima are caused by non-smooth changes in the power generation. However, both process configuration 2 and 3 are rather flat with respect to changes in the feed temperature at high tail gas recycle ratios

Fig. 9 shows the required palladium membrane area for process configurations 2 and 3. As we can see, process configuration 3 has always a lower membrane area, independently of the tail gas recycle ratio and the temperature to the last WGS reactor. This is caused by the higher feed temperature to the palladium membrane modules, counteracting the increased flowrates to the module. Increasing the tail gas recycle ratio has only a negligible impact up to a recycle ratio of around 90 % from which point onwards, we can see an exponential increase due to the exponential increase in the feed flowrate. It is interesting to note that the impact of the WGS feed temperature is small in process configuration 3 compared to process configuration 2. As process configuration 3 does not include a HT-WGS reactor, we have an increased conversion in the MT-WGS reactor compared to the conversion in the LT-WGS reactor in process configuration 2. Correspondingly, process configuration 3 has always a higher outlet temperature of the WGS reactor, and hence, a higher feed temperature to the palladium membrane. The flux through the palladium membrane increases however only marginally above a certain temperature. Hence, the increase in the outlet temperature of the MT-WGS reactor does not give a similar reduction in membrane area as it is the case for process configuration 2.

3.2 Improved process parameters for CO_2 separation

The sensitivity analysis in the previous sections were conducted using fixed parameters in the CO_2 liquefaction section. The main

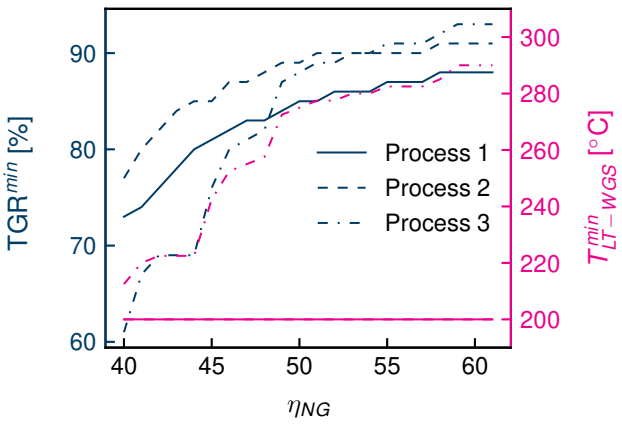

Fig. 8 Tail gas recycle ratio (TGR) and feed temperature to the LT-WGS reactor ($LT-WGS$) at the minimum in the specific equivalent power input as a function of the turbine efficiency η_{NG} for the different process configurations.

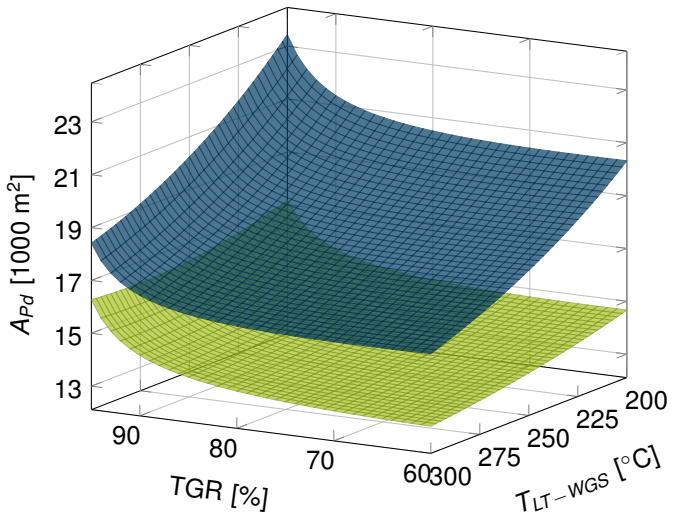

Fig. 9 Palladium membrane area as a function of tail gas recycle ratio and LT–WGS inlet temperature. Process configurations 2 and 3 are represented by blue and green surfaces, respectively. The reader is referred to the web version for colour coding.

separation was conducted at a pressure of 80 bar and a temperature of −54 °C while the purification in the third flash unit was conducted at a pressure of 6 bar and a temperature of −55 °C.

The liquid yield and CO_2 cut achieved in the main separator is highly dependent on the separation temperature and pressure as well as feed CO_2 concentration and overall composition. This is shown using the CO_2 cut in the supplementary information†. Furthermore, these parameters have a major influence on the operating costs of the CO_2 capture system. A lower pressure and a higher temperature results in reduced operating costs but at the expense of a reduced separation efficiency. Due to the recycle of the tail gas to the water–gas shift section, the impact of the reduced pressure and temperature on the total CO_2 capture ratio may be reduced. However, there exists a minimum with respect to operating costs due to the increased flow in the recycle loop. Hence, it is necessary to identify systematically the best operating conditions. Further important process parameters are the heat duty in the intermediate temperature auxiliary refrigeration loop and the pressure of the high pressure propane loop. The latter has an influence on the size of the heat sink heat exchanger in the refrigeration loop and the compressor size and energy requirement. The following illustrations are related to process configuration 2. Both process configurations 1 and 3 behave similar to process 2 with only changes in the absolute values and slight changes in the position of the minima. Corresponding figures can be found in the supplementary information†.

Fig. 10 visualizes the specific equivalent power requirement v_R for changes in the separation pressure and temperature. From this plot, it is possible to see a minimum for the separation pressure for a given separation temperature. A key point is that neither a very low separation temperature at a low separation pressure nor a very high separation temperature at a high separation pressure is desirable for the energy demand. Note that although the difference of 0.09 kWh/kg H_2 between the maximum and minimum value in the chosen range seems small and corresponds to 0.37 %, it corresponds to a reduction in the energy demand of the separation of 20.66 %. This is caused by the large demand for energy in the form of natural gas.

Fig. 11 shows the corresponding CO_2 capture ratio. It is not surprising that the CO_2 capture ratio is increasing with both a higher separation pressure and and lower temperature. The actual increase is however interesting to see, as the change is only 1.5 pp from the lowest to the highest capture ratio. Furthermore, the CO_2 capture ratio shows a constant reduction in the marginal increase through higher separation pressure and lower temperature. This increase essentially is negligible at low temperatures and high pressures. Fig. 12 summarizes Fig. 10 and Fig. 11. Here, the sensitivity data is utilized to plot the CO_2 capture ratio as a function of the specific equivalent power input at a constant temperature. From this plot, it can be seen that the indicated optimum with respect to pressure at each temperature is on a pareto front. That implies that the optimal separation temperature and pressure with respect to v_R can be identified for a chosen CO_2 capture ratio. The following analysis of process parameters will therefore use a separation temperature of −47 °C and pressure of 55.0 bar. These conditions correspond to an acceptable reduction in the CO_2 capture ratio (CO_2 capture ratio > 96 %) while reducing the energy demand of the liquefaction.

A second important point for improving the performance of the separation section is the distribution of the cooling duties in-between the two auxiliary refrigeration loops in Fig. 3. The initial outlet temperature of the IT refrigeration loop is set to −12 °C. This corresponds to a distribution of the cooling duty of 28 % to the IT refrigeration loop and 14 % to the LT refrigeration loop while the remaining cooling of the CO_2-rich feed stream is achieved through heat integration in the multistream heat exchangers. The refrigeration cycle in itself is responsible for 44 % of the total energy demand in the liquefaction section. Fig. 13 shows the energy demand of the liquefaction section and the specific equivalent power requirement as a function of the

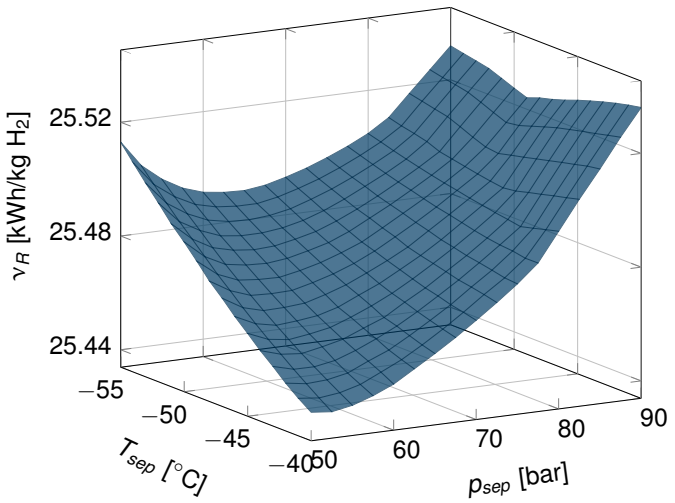

Fig. 10 Specific equivalent power input as a function of the separation temperature T_{Sep} and pressure p_{Sep} for process configuration 2.

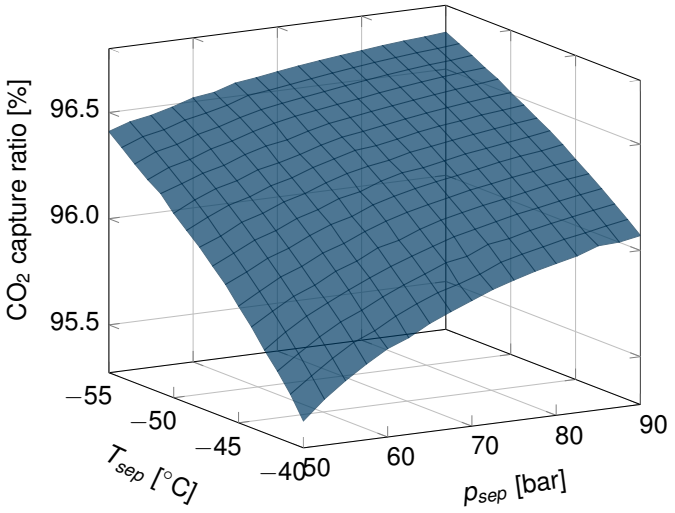

Fig. 11 CO_2 capture ratio as a function of the separation temperature T_{Sep} and pressure p_{Sep} for process configuration 2.

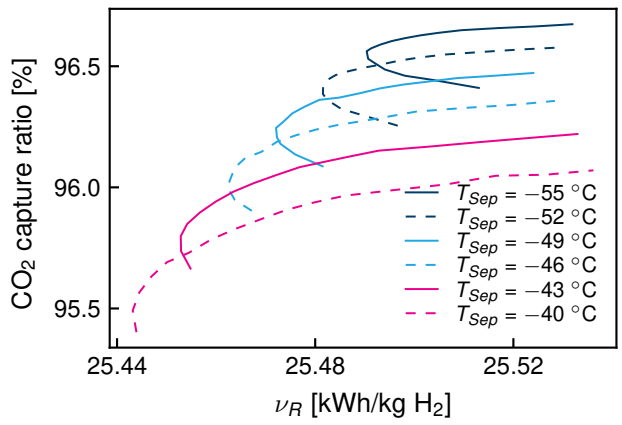

Fig. 12 CO_2 capture ratio as a function of the specific equivalent power input at constant temperatures T_{Sep} for process configuration 2. The reader is referred to the web version for colour coding.

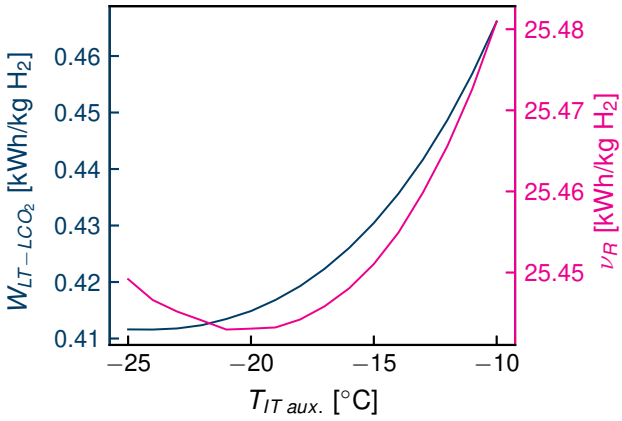

Fig. 13 Specific energy demand of liquefaction section (left axis) and the specific equivalent power requirement (right axis) as a function of the outlet temperature of the IT refrigeration loop for process configuration 2. The reader is referred to the web version for colour coding.

outlet temperature of the IT refrigeration loop. We can see, there is a clear optimum with respect to the outlet temperature of the IT refrigeration loop for each of the different process configurations. This optimum is however different for the specific power requirement of the liquefaction section and the specific equivalent power consumption ν_R. The former has a minimum at −24 °C while the latter has a minimum at −21 °C. Furthermore, the reduction in equivalent power consumption is reduced compared to the reduction in the power requirement of the liquefaction section. This is caused by a reduction in the flowrate to the furnace, and hence, a reduction in the power generated in the steam turbines. For the overall process, it is beneficial to use a temperature of −21 °C. The new distribution in cooling duties is then given by 41 % to the IT refrigeration loop and 7.1 % to the LT refrigeration loop. The contribution of the refrigeration loop is increased to 46 % of the energy demand of the liquefaction section. The total cooling demand is however reduced and the higher cooling duty in the IT refrigeration loop compared to the LT refrigeration loop reduces the overall energy demand due to a higher coefficient of performance in the IT refrigeration loop.

The power requirement of the liquefaction can be further reduced by changing the high pressure (HP) in the propane cycle of the refrigeration cycle in Fig. 4. An increase in the pressure will result in a reduction in the area of the following heat exchanger and an increase in the compression power requirement. Hence, it can be expected that the overall capital costs are expected to remain rather flat with reducing the high pressure. This change will only affect the compressor and heat sink in the refrigeration loop. The the specific compressor duty as a function of high pressure of the propane cycle. A lower limit of 9.5 bar is close to the minimum pressure at which sufficient cooling can be achieved with the Joule-Thompson effect in the subsequent valve. The compressor duty is reduced almost linearly with a reduction in pressure. Hence, it is beneficial to operate at the minimum pressure of 9.5 bar.

3.3 Final process parameters

Table 5 summarizes the best process parameters and the corresponding KPIs. Based on the analysis in the previous section, process configurations 1 and 2 were adjusted to a carbon capture ratio of around 96 %. Process configuration 3 was adjusted to a CO_2 capture ratio of 94 % as higher capture ratios are difficult to obtain due to the relatively high concentration of CO. This resulted in a lower feed temperature to the LT–WGS reactor to increase CO conversion than the identified in Fig. 8. The chosen carbon intensity of the electricity grid is 18.9 $\frac{\text{kg CO}_2}{\text{MWh}}$ which corresponds to the emission intensity in the Norwegian electricity grid. Due to the different configurations, $\Delta Q_{rel,LT-LCO_2}$ for process configuration 1 is relative to a tail gas recycle of 60 % and a feed temperature of 200 °C in process configuration 1.

As we can see from Table 5, process configuration 2 has the highest energy efficiency and lowest ν_R. Process configuration 1 has a slightly higher CO_2 capture ratio than process configuration 2, and hence, a smaller σ_r. Furthermore, process configuration 1 is different as there exists an unconstrained minimum ν_R for variations in the separation pressure and temperature, contrary to the other two process configurations. The lower tail gas recycle ratio in process configuration 1 can be explained by the higher impact of the tail gas recycling on the energy demand as more compression steps are required. Process configuration 3 is different due to the single water–gas shift reactor. Especially the CO_2 capture ratio is comparably low due to unreacted CO. However, the energy efficiency is higher than for process configuration 1. The key aspect is however the 27.5 % reduction in size of the palladium membrane compared to process configuration 2, implying a significant cost reduction. Fig. 9 shows that an increase in the temperature to the low temperature water–gas shift reactor reduces the required size of the palladium membrane as it increases the outlet temperature. However, even at a feed temperature of 300 °C and a tail gas recycle ratio of 89 %, the required area is still 16646 m^2 for process configuration 2, slightly higher than process configuration 3, and at the cost of a reduced CO_2 capture ratio of 94.4 %. The corresponding first law energy efficiency η_R^{HHV} is then given by 84.37 %. Hence, it may be still a valid option.

Table 5 Final process parameters chosen for the different process configurations

Parameter	Unit	Process 1	Process 2	Process 3
TGR	%	88	91	92
T_{Feed}	°C	200	200	225
T_{sep}	°C	−51	−47	−46
p_{sep}	bar	67.5	55	60
$T_{IT\,aux.}$	°C	−19	−21	−21
p_{HP}	bar	9.5	9.5	9.5
CCR	%	96.38	96.08	94.07
σ_R	$\frac{\text{kg CO}_2}{\text{kg H}_2}$	0.30	0.32	0.50
η_R^{HHV}	%	83.61	84.74	84.08
η_R^{LHV}	%	78.18	79.28	78.64
ν_R	$\frac{\text{kWh}}{\text{kg H}_2}$	25.86	25.41	25.67
A_{Pd}	m^2	–	22129	16054
$\Delta Q_{rel,NG}$	%	−3.02	−3.84	−3.33
$\Delta Q_{rel,LT-WGS}$	%	4.77	4.19	10.21
$\Delta Q_{rel,LT-LCO_2}$	%	7.37[1]	17.77	40.86

[1] Relative to process 1 with a TGR of 60 % and a feed temperature of 200 °C.

4 Discussion

Section 3 showed that tail gas recycling to the water–gas–shift reactor has an important impact on both the environmental footprint and the economics of natural gas reforming. In fact, both the energy efficiency and carbon capture ratio increase up to a very high recycle ratio.

However, the improved performance of the reforming process comes at the price of 1. increased equipment size for the water–gas shift reactor and the separation section, and 2. reduced power generation in the steam turbine.

4.1 Increased equipment size

As shown in Fig. 14 for process configuration 2 and in Table 5 for the chosen process parameters, tail gas recycling affects the volumetric flows, and hence, costs and size of required equipment. Due to the process layout, the impact of the tail gas recycling is different for the different sections of the process. The feed to the last water–gas shift reactor (pink in Fig. 14) is only moderately increased, especially when compared to the reduction in the natural gas feed for process configuration 2. The same holds true for process configuration 1 (figure shown in the supplementary information). Process configuration 3 (figure shown in the supplementary information) however has a quite large increase in the volumetric flow rates at moderate tail gas recycles resulting in increased equipment costs compared to the other two configurations. Similarly, the size of the hydrogen separation units changes only moderately. On the other hand, there is a significant increase in flow rate to the low temperature liquefaction section of up to 30 % (green in Fig. 14). Especially at high tail gas recycle ratios, the impact of increased flow rate on the increase in the investment costs will depend on the cost scaling exponents of the equipment.

However, tail gas recycling reduces the required natural gas feed (dark blue in Fig. 14) for a fixed production volume which is also represented by the increased energy efficiency shown in Fig. 6. That implies that the size of all equipment located before the last water–gas shift reactor is reduced. Hence, it cannot be directly said if the investment costs are higher than in the case without tail gas recycling. To this end, it is necessary to conduct a detailed techno–economic analysis of the different tail gas recycle ratios to see the real impact on the investment costs. A second aspect to consider is the impact of the reduced natural gas consumption on the hydrogen production costs. The hydrogen production cost is dominated by the cost of natural gas, even when considering low natural gas prices[24]. This is even more pronounced when considering today's natural gas prices in Europe. In addition, natural gas prices can vary significantly depending on the location of the hydrogen production plant, complicating the calculations even further. Hence, the impact of tail gas recycling on the hydro-

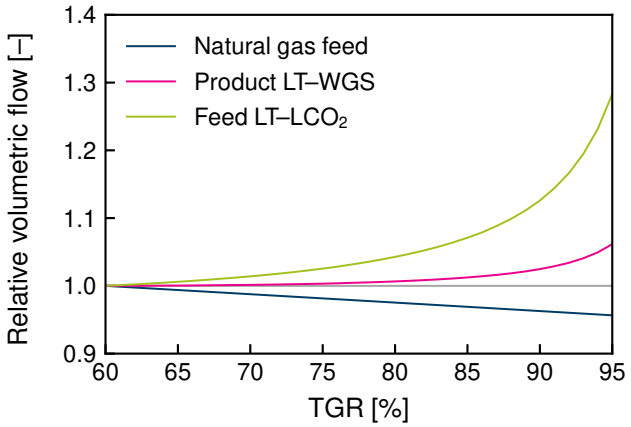

Fig. 14 Relative volumetric flows for process configuration 2 and a feed temperature to the LT–WGS reactor of 200 °C. The grey line corresponds to a constant value of 1.0. The reader is referred to the web version for colour coding.

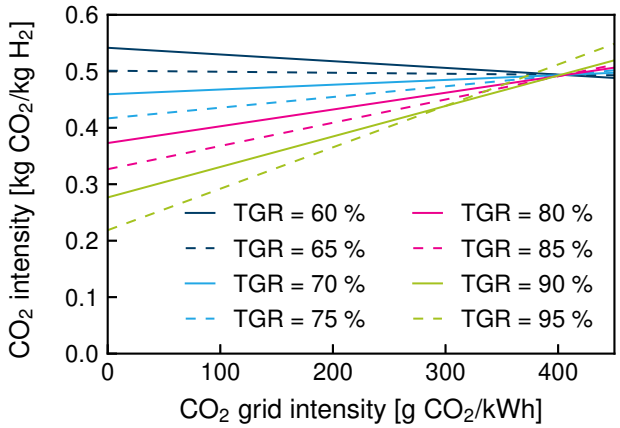

Fig. 15 CO_2 intensity of hydrogen as a function of the CO_2 intensity of the electric grid for process configuration 2 and a feed temperature to the LT–WGS reactor of 200 °C. The reader is referred to the web version for colour coding.

gen production costs is beyond the scope of this work and will be investigated in a future work.

4.2 Reduced electricity generation

The overall process moves from net electricity generation to requiring electricity from the electrical grid. This is mostly caused by a reduction in tail gas sent to the furnace, and hence, in electricity generation in the steam cycle. The burning of the remaining tail gas serves therefore more like a purge stream, avoiding the build-up of inerts like unreacted methane. However, the gross electricity demand of the process is reduced up to a minimum between 70 % and 85 % depending on the process configuration. Increasing the tail gas recycling ratio further results in an initially small increase which is substantial after a recycle ratio of around 90 %. Hence, if the surplus heat is not used for electricity generation in a steam cycle, it will be always beneficial to utilize an increased tail gas recycle. Not utilizing the surplus heat comes however at the cost of a reduced energy efficiency.

Depending on the source of the electricity and the resulting CO_2 grid intensity, the increase in net electricity demand of the process may increase the carbon intensity of the produced hydrogen counteracting the reduction in carbon intensity of the reforming process. Fig. 15 shows the CO_2 intensity of the produced hydrogen as a function of the CO_2 grid intensity. As we can see, a very high tail gas recycle of 95 % is beneficial up to a CO_2 grid intensity of around 270 g CO_2/kWh, beyond which a reduced tail gas recycle ratio is better. Furthermore, it is interesting to note that the CO_2 intensity of hydrogen is quite similar for all tail gas recycle ratios at a CO_2 grid intensity of 390 g CO_2/kWh. Note that the net electricity generating cases with a tail gas recycle ratio of up to 65 % have a reduced CO_2 intensity with an increased CO_2 grid intensity. The generated electricity counts with the emission factor of the electricity grid, and therefore, reduces the CO_2 emissions of hydrogen with increasing CO_2 grid intensity as it feeds electricity to the grid.

An additional means for reducing the demand for electric power is to optimize the cryogenic air separation unit for the required delivery pressure. In the current configuration oxygen is assumed to be supplied at atmospheric pressure and subsequently compressed in three stages. A tailored unit could pressurise the O_2 by liquid pumping prior to heating in the front-end multi-stream heat exchanger in the cryogenic unit, potentially reducing the overall power demand for oxygen supply.

The reduced electricity generation, and hence, increased electricity demand also has an impact on the production costs. The electricity prices currently observed in Europe may impact the eventual design choice. It may be hence economically better to utilize a lower recycle ratio depending on the relationship between the natural gas and electricity prices.

4.3 Application of liquefaction for separation

Direct liquefaction of CO_2 as separation technology only applies standard equipment already in use in cryogenic processes. Hence, there are no technical barriers to be overcome or new equipment types to be developed for realizing low–temperature CO_2 liquefaction and separation. The component design and materials need to be rated for this specific purpose, but can be fully derived from existing technologies. Thus the main innovation lies in the process design and integration of the liquefaction process and its integration with the complementary hydrogen purification technology and water–gas shift reactor.

As an example of component availability, far more advanced cryoexpanders are in use in cryogenic disciplines than what is needed in the low-temperature CO_2 liquefaction unit. Radial turboexpanders with dynamic gas bearing are in use in hydrogen liquefiers, with isentropic efficiencies above 85 % for specific enthalpy drops above 90 kJ/kg[25]. The expanded tail gas in the CO_2 liquefaction process has considerably higher molecular mass, lower specific enthalpy drop and substantially less demanding temperature levels than in the hydrogen liquefaction application.

Regarding the practical applicability of the low-temperature separation principle, Trædal *et al.*[26] verified simulation results

for low-temperature liquefaction and separation of CO_2 from a binary CO_2/N_2 mixture. The experiments were executed in a scale of approximately 6 t/d feed flowrate and with two separation vessels in sequence, that is, a simplified configuration of the process schemes presented in this paper. Results based on measurements of flowrate, temperature, pressure and composition verified expectations for CO_2 liquid yield as well as purity of the final CO_2 product. In the experiments, average liquid retention time was in the range 36–80 s. The experimental pilot setup is currently upgraded to handle gases like H_2, CH_4, and CO in order to run corresponding experiments relevant to the feed conditions typical for the duties given in this work. Once the setup is upgraded, it is possible to verify the results of the liquefaction process as complementary CO_2 separation and CO recovery technology in low–emission hydrogen production.

In the low-temperature capture unit, CO_2 is pressurized to high-pressure pipeline conditions by liquid pumping with extremely low additional power requirement. The advantage of utilizing CO_2 liquefaction technology is especially pronounced when it is desirable to transport CO_2 in liquid form by ship, since the CO_2 can be made readily available in cold liquid form at the required pressure level for the given ship transport condition. Ship transport of CO_2 is likely to be important as it can lower the threshold for realizing full-scale CCS chains. This is for example the case in the Norwegian Northern Lights project, which will rely on ship transport of liquid CO_2 [27]. Since the low-temperature processing unit is flexible with respect to final state of CO_2, it can be designed with the option of quick conversion from any early-phase transport state, *e.g.* , liquid CO_2 at 16 bar pressure, *via* a mid-phase state, *e.g.* , liquid CO_2 at 6 bar pressure, eventually to high-pressure CO_2 after investments in pipeline transport have been made.

4.4 Further increase in CO_2 capture ratio

As shown in the Section 3, increasing the CO_2 capture ratio further comes at increased electricity demand and equipment size. These increases are mostly caused by 1. a build-up of inert species in the recycle loop for high tail gas recycle and 2. by a decreased liquefaction temperature and increased liquefaction pressure. However, there is a technical limit caused by the source of the CO_2 emissions, that is in which stream and in which form it is emitted.

As we can see from Table 6, only 35 % of emitted CO_2 is in the form of CO_2 in the tail gas to furnace stream, whereas the remainder is in the form of CO and CH_4. The amount of CO can be reduced through a lower feed temperature to the low temperature water–gas shift reactor or utilizing even more stages. However, as the molar concentration of CO in the outlet of the LT–WGS reactor in process configuration 2 with a tail gas recycle of 91 % and a feed temperature of 200 °C is only 1.1 %, it may be not feasible to reduce the CO concentration further at reasonable costs. Similarly, problems arise with CH_4. CH_4 as source can be reduced through a higher conversion in the autothermal reformer, *e.g.* , through a higher reactor temperature or different steam to carbon ratios. Both will however have an impact on the overall process performance. The current conversion of methane is 98.6 %, reducing the viability of a reduction. The last emission source is dissolved CO_2 in the water before or after the separation of hydrogen as the separation of water is achieved at ambient temperature and elevated pressure. This emission source can be reduced through flashing the water. To summarize, most of the emitted CO_2 is not in the form of CO_2 in the tail gas to the furnace. Instead, it is necessary to modify process parameters in the low temperature water–gas shift and autothermal reactor, respectively.

Table 6 Source for and percentage of emitted CO_2 in the case of process configuration 2 at the conditions outlined in Table 5.

Stream	Form	Percentage
Water (Fig. 3)	CO_2	21
Tail gas to furnace (Fig. 2 b))	CO	14
	CO_2	35
	CH_4	30

4.5 Comparison to reported data

IEAGHG [21] reports a lower heating value efficiency of 69 %, a carbon capture ratio of 90 %, and a carbon intensity of 1.0 $\frac{\text{kg } CO_2}{\text{kg } H_2}$. If we compare these numbers with Table 5, we can see that they are worse in every aspect. The increase in the carbon capture ratio from 90 % to 96 % reduces the associated CO_2 emissions drastically. Similarly, the reported efficiency value is 9–10 percentage points lower.

The main reason for the observed differences can be explained by the choice of reactor and separation technology. IEAGHG utilizes a steam methane reformer with flue gas capture from the furnace of the reactor. This is disadvantageous as the partial pressure of CO_2 is low in this stream while the volumetric flow is generally large. Consequently, the absorber has to be be large for a sufficient high capture ratio. In addition, only a high temperature water–gas shift reactor is used. This may be advantageous in the context of hydrogen production without CO_2 capture to utilize the CO for heating and to reduce capital costs. However, when CO_2 capture is used, it has the disadvantage that a significant fraction of potential hydrogen is lost in the form of CO as shown by Antonini *et al.* [20]. This shows that both the proper selection of reactor and corresponding separation technology is important for achieving a high efficiency coupled with a high CO_2 capture ratio.

5 Conclusion

In this paper, we propose the utilization of a new CO_2 capture process in combination with hydrogen–selective syngas separation and tail gas recycle for hydrogen production from natural gas with extremely low CO_2 emissions. The direct utilization of CO_2 liquefaction allows a tighter integration of the CO_2 capture process into the hydrogen production compared to conventional amine scrubbing or other solvent processes. This integration results in both an increased energy efficiency and an increased global carbon capture ratio.

It is possible to obtain very high carbon capture ratios without a drastic increase in the electricity consumption. The resulting CO_2 intensity is very low. The CO_2 intensity of the production and transport of natural gas in itself is already higher than the CO_2 intensity of the hydrogen production process[7].

Author Contributions

Conceptualization: RA, DB; Formal Analysis: JS, VTS; Investigation: JS, VTS; Methodology: JS; Project Administration: DB; Supervision: RA, DB; Validation JS, RA, DB; Visualization: JS; Writing – original draft: JS; Writing – review & editing: RA, VTS, DB

Conflicts of interest

JS and DB are the inventors of a patent related to the proposed process.

Notes and references

1 Hydrogen Council, *Hydrogen scaling up. A sustainable pathway for the global energy transition*, Hydrogen council technical report, 2017.

2 IEA, *Net Zero by 2050*, International Energy Agency technical report, 2021.

3 G. S. Seck, E. Hache, J. Sabathier, F. Guedes, G. A. Reigstad, J. Straus, O. Wolfgang, J. A. Ouassou, M. Askeland, I. Hjorth, H. I. Skjelbred, L. E. Andersson, S. Douguet, M. Villavicencio, J. Trüby, J. Brauer and C. Cabot, *Renewable and Sustainable Energy Reviews*, 2022, **167**, 112779.

4 IEA, *The Future of Hydrogen. Seizing today's opportunities*, International Energy Agency technical report, 2019.

5 IEA, *Global Hydrogen Review 2021*, International Energy Agency technical report, 2021.

6 D. Jansen, M. Gazzani, G. Manzolini, E. van Dijk and M. Carbo, *International Journal of Greenhouse Gas Control*, 2015, **40**, 167 – 187.

7 F. Ueckerdt, P. C. Verpoort, R. Anantharaman, C. Bauer, F. Beck, T. Longdon and S. Roussanaly, *On the cost competitiveness of blue and green hydrogen*, Preprint submitted to Nature Energy, available from `https://doi.org/10.21203/rs.3.rs-1436022/v1`, 2022, Accessed: 2022-08-30.

8 H21, *H21 North of England*, Equinor Technical Report H21 NoE Report/2018, 2018.

9 H. Malerød-Fjeld, D. Clark, I. Yuste-Tirados, R. Zanón, D. Catalán-Martinez, D. Beeaff, S. H. Morejudo, P. K. Vestre, T. Norby, R. Haugsrud, J. M. Serra and C. Kjølseth, *Nature Energy*, 2017, **2**, 923–931.

10 D. Kim, D. Berstad, R. Anantharaman, J. Straus, T. A. Peters and T. Gundersen, *30th European Symposium on Computer Aided Process Engineering*, Elsevier, 2020, vol. 48, pp. 445–450.

11 S. M. Nazir, J. H. Cloete, S. Cloete and S. Amini, *Energy*, 2019, **185**, 372–385.

12 M. Voldsund, K. Jordal and R. Anantharaman, *International Journal of Hydrogen Energy*, 2016, **41**, 4969–4992.

13 J. A. Ritter and A. D. Ebner, *Separation Science and Technology*, 2007, **42**, 1123–1193.

14 F. Gallucci, E. Fernandez, P. Corengia and M. van Sint Annaland, *Chemical Engineering Science*, 2013, **92**, 40 – 66.

15 N. Al-Mufachi, N. Rees and R. Steinberger-Wilkens, *Renewable and Sustainable Energy Reviews*, 2015, **47**, 540 – 551.

16 C. Antonini, J.-F. Pérez-Calvo, M. van der Spek and M. Mazzotti, *Separation and Purification Technology*, 2021, **279**, 119715.

17 D. Berstad, R. Anantharaman and P. Nekså, *International Journal of Refrigeration*, 2013, **36**, 1403 – 1416.

18 K. Jordal, R. Anantharaman, T. A. Peters, D. Berstad, J. Morud, P. Nekså and R. Bredesen, *Energy*, 2015, **88**, 9–17.

19 K. Aasberg-Petersen, I. Dybkjær, C. Ovesen, N. Schjødt, J. Sehested and S. Thomsen, *Journal of Natural Gas Science and Engineering*, 2011, **3**, 423–459.

20 C. Antonini, K. Treyer, A. Streb, M. van der Spek, C. Bauer and M. Mazzotti, *Sustainable Energy & Fuels*, 2020, **4**, 2967–2986.

21 IEAGHG, *Techno-Economic Evaluation of SMR Based Standalone (Merchant) Hydrogen Plant with CCS*, IEA GREENHOUSE GAS R&D PROGRAMME Technical Report 2017/2, 2017.

22 D. O. Berstad, Ø. Wilhelmsen, V. T. Skjervold and P. Nekså, Refrigeration Science and Technology, 2017, p. 158 – 164.

23 O. Fandiño, J. M. Trusler and D. Vega-Maza, *International Journal of Greenhouse Gas Control*, 2015, **36**, 78 – 92.

24 UK Department for Business, Energy & Industrial Strategy, *Hydrogen Production Costs 2021*, UK Department for Business, Energy & Industrial Strategy technical report, 2021.

25 S. Bischoff and L. Decker, *AIP Conference Proceedings*, 2010, **1218**, 887–894.

26 S. Trædal, D. Berstad and J. Stang, Refrigeration Science and Technology, 2019, pp. 147–153.

27 Equinor, *Northern Lights Project Concept report*, Equinor Technical Report RE-PM673-00001, 2019.